




Blood metal analysis of plasmas from donors with and without SARS-CoV-2 using laser-induced breakdown spectroscopy and logistic regression

NOUREDDINE MELIKECHI,^{1,*}  HELMAR G. ADLER,¹ ALI SAFI,¹  JOSHUA E. LANDIS,¹ FARHAD POURKAMALI-ANARAKI,^{1,2}  KEMAL EFE ESELLER,^{1,3} KIM BERLO,⁴ DANIELLE BONITO,⁵ GREGORY R. CHIKLIS,⁵ AND WEIMING XIA^{1,6,7}

¹Kennedy College of Sciences, University of Massachusetts Lowell, Lowell, MA 01854, USA

²Present address: University of Colorado Denver, Denver, CO 80204, USA

³Department of Electrical - Electronics Engineering, Atılım University, 06836, Ankara, Turkey

⁴Department of Earth & Planetary Sciences, McGill University, Montreal H3A 0E, Canada

⁵MRN Diagnostics, 101 Constitution Blvd, Franklin, MA 02038, USA

⁶Bedford VA Healthcare System, Bedford, MA 01730, USA

⁷Boston University Chobanian & Avedisian School of Medicine, Boston, MA 02118, USA

*Nouredine_Melikechi@uml.edu

Abstract: Research on the correlation between metal levels in blood and Covid-19 infection has been conducted primarily by assessing how each individual blood metal is linked to different aspects of the disease using samples from donors with various levels of severity to Covid-19 infection. Using logistics regression on LIBS spectra of plasma samples collected pre- and post-Covid-19 pandemic from donors known to have developed various levels of antibodies to the SARS-Cov-2 virus, we show that relying on the levels of Na, K, and Mg together is more efficient at differentiating the two types of plasma samples than any single blood alone.

© 2023 Optica Publishing Group under the terms of the [Optica Open Access Publishing Agreement](#)

1. Introduction

In December 2019, the world experienced a sudden outbreak of a pandemic caused by the severe acute respiratory syndrome coronavirus 2 (SARS-CoV-2). This pandemic led to the death of over six million people worldwide [1], and a significant loss in the world-wide gross domestic product [2]. Based on thousands of studies published since the pandemic started [3], we have a greater understanding of disease progression, and more effective means to improve patient's lives. Several blood metals were considered. For example, Sklany *et al.* reported that, compared to controls, the severity of Covid-19 was associated with a decrease in the serum levels of Ca, Fe, Se, and Zn, whereas serum Cu and especially Cu/Zn ratio were elevated [4].

Reports on the relationship between blood metals and the health status of Covid-19 patients are mostly focused on the severity of the disease. Noori *et al.* have observed in Covid-19 both lower and higher deviations of K levels from the normal range [5]. Similarly, Yasari *et al.* have noted that in terms of the role of K on the severity of Covid-19, their study was not conclusive and suggested that further studies be conducted [6]. By evaluating the electrolyte imbalances of 286 Covid-19 patients, Taci Hoca and Berktaş reported that hypocalcemia (lower levels of Ca than normal) and hyponatremia (lower levels of Na than normal) effectively predicted disease progression to severity [7]. Taking a broader view, Song *et al.* conducted a comprehensive analysis of 28 independent observational studies that consisted of a total of 26,897 Covid-19 patients [8]. Part of this study focused on looking at the connection of electrolytes imbalances and clinical outcome and showed that hyponatremia, hypernatremia (higher levels of Na than

normal), as well as hypocalcemia to be associated with significant enhancement of severity of the disease. Studies have also suggested an increased Covid-19 severity for patients with some imbalances in serum electrolytes and glucose levels. Lippi *et al.* reported that Covid-19 severity is associated with lower serum concentrations of Na, K, and Ca [9]. Micke *et al.* suggested that Mg deficiency could be one of the risk factors for severe Covid-19 as it may decrease the resistance against infection with the coronavirus 2 [10]. Trapani *et al.* tried to explore if Covid-19 infection lowers Mg levels [11], while Iotti *et al.* investigated the role of Mg during the viral infection [12]. Other chemical elements, such as Cu and Se, and Zn have also been considered either as potential agents against Covid-19 or as part of an adjunct therapy treatment for severe Covid-19 patients [13–17]. For example, Sarvazad *et al.* investigated Mg, K, Na, and glucose concentration in sera of 134 patients with various degrees of severity of Covid-19 [17]. Chen *et al.* reported the prevalence of hypokalemia (low levels of K) among patients with Covid-19 [18]. Recently, two research groups have also focused on the relationship between the severity of Covid-19 and the levels of trace elements in sera [19–20]. Our research group reported on an investigation based on using Laser-induced breakdown spectroscopy (LIBS) and Inductively Coupled Plasma- Mass Spectroscopy (ICP-MS) of blood plasma samples of donors who tested positive for SARS-CoV-2 and healthy controls [21]. This study corroborated the importance of individual bio metals in distinguishing samples as noted by previous research groups [9,17]. However, it did not investigate the impact of the combined effect of multiple blood metals on the differentiation of plasma samples from Covid-19 free donors collected pre-pandemic and those donors infected with SARS-CoV-2.

Studies on changes in metals in blood among Covid-19 positive donors have been performed by looking at the effect of individual bio-metal on aspects of the disease, mostly on its severity. To the best of our knowledge, no study has been conducted on the levels of blood metals in Covid-19 patients by considering combinations of multiple blood metals measured simultaneously in plasmas collected pre- and post- pandemic. Yet, one of the hallmarks of the effects of multiple metals present in blood is their complex role in a myriad of biomedical mechanisms. Their interdependent interactions complicate our understanding of the biochemical processes. To obtain more clarity, the focus should not lie solely on the role of individual metals but on the impact of their associations and relations on the disease. Due to their ability to reveal information “hidden” in large sets of data of biomedical samples and most notably to compare samples of diseased patients to controls, machine learning algorithms have evolved to become useful tools [22–28].

In this study, we used LIBS to search for potential associations between levels of blood metals in plasma samples collected before December 2019, in other words pre-pandemic (used as healthy controls) and post-Covid pandemic (known to have been infected with SARS-CoV-2) irrespective of the severity of the Covid-19 disease. Using LIBS spectra of the two types of plasma samples, we have identified Na, K, Mg, and Ca as the blood metals that have the potential to differentiate the plasma samples from healthy controls and those known to have been infected with the SARS-CoV-2 virus. The Covid-19 status of the donors was checked by RT-PCR and confirmed by measuring the IgG values for all the samples using the LumiraDx SARS-CoV-2 antigen microfluidic immunofluorescence assay [29]. We have measured the LIBS spectra of the two groups of plasma samples and analyzed them using logistic regression analysis. In this study, we opted for LIBS because it allows to acquire, rapidly and simultaneously, the multi-elemental composition of the plasma samples without the necessity for their preparation.

2. Methods

2.1. Sample preparation

We have acquired LIBS spectra of the plasma samples of 150 donors. These consist of 46 pre-Covid-19 pandemic samples (we refer to these as *negative* samples), used as healthy controls,

64 post- SARS-CoV-2 pandemic samples confirmed by reverse transcription-polymerase chain reaction (RT-PCR) to have been infected by the SARS-CoV-2 (we refer to these as *positive* samples). The remaining 40 samples, whose Covid-19 status was unknown to the researchers performing the spectroscopic studies, were referred to as *blind* samples.

We used the same protocol for sample collection, processing, storage, and spectroscopic measurements for all three classes of blood samples: negative as healthy controls, positive known to have contracted the SARS-CoV-2 virus and the blind samples. The blood samples of the three classes of donors were collected, processed, and stored using the same procedure. The blood samples were collected under the National Expanded Access protocol sponsored by the Mayo Clinic. Sample collection was also approved by the MRN Diagnostics Institutional Review Board. Informed consent was obtained from all subjects and studies were performed in accordance with FDA guidelines and regulations including IRB approval. Blood was drawn from donors by venipuncture in a heparinized tube. The candidates for this study were recruited in the Boston or Florida area by self-referral or by their own interest in knowing their Covid status. Enrollment criteria included men and women, aged 18-81, and a mix of blood types. The description of the characteristics of the donors is provided in [Supplement 1 \(S1\)](#).

Plasma was separated by centrifugation within 30 min of blood collection and stored for up to 4 weeks at $\leq -10^{\circ}\text{C}$ followed by long term storage at $\leq -70^{\circ}\text{C}$. The samples were collected in sodium citrate anticoagulant from donors drawn by MRN Diagnostics both before (pre 11/2019) and after the appearance of SARS-CoV-2 in the United States. All samples were previously thawed once on ice for making aliquots. The Si wafer (100 mm in diameter, type N, and 500 μm thick, University Wafer) used as a substrate had small intrusions to retain the liquid plasma samples. The Si wafer was rinsed three times with isopropanol. 2 μl of each sample was pipetted, gently shook for few seconds, and deposited onto the Si substrate, and dried with a lamp. To reduce the possibility of systematic errors and bias, the three classes of samples were randomly placed on the substrate and then dried using an infrared lamp light for 10 minutes. In addition to PCR, we checked whether our samples were negative or positive using a LumiraDx SARS Cov-2 antigen microfluidic immunofluorescence assay with a quantitation card provided by LumiraDx to follow antibody levels against each of their antigens in the test strip. It is important to mention that the LIBS investigators were unaware of the RT-PCR results of the blind samples prior to completing the LIBS analysis. Subsequently, we further verified the Covid-19 status of each patient by employing the LumiraDx SARS-CoV-2 antigen microfluidic immunofluorescence assay.

2.2. Experimental method

LIBS is an analytical method that provides emission spectral lines characteristics of a sample [30–32]. It is based on the use of a laser intense enough to create a plasma on the surface of a sample to be investigated. As the plasma cools down it emits radiation characteristics of the sample which can be analyzed to obtain the composition of the sample. LIBS has been used in numerous including biomedical applications and provides numerous advantages such as the ability to yield rapidly multi-elemental qualitative and quantitative information with no or minimal sample preparation [33–35]. An additional advantage of using LIBS for the present study is its minimal sample volume which can be performed by drying a blood plasma droplet on a silicon substrate. Other researchers have conducted LIBS measurements in liquids using metallic substrate [36].

To obtain the LIBS spectra of the blood plasma samples, a Q-switched Nd-YAG laser (Continuum, Surelite II), operating at 1064 nm, a repetition rate of 0.5 Hz, a laser energy of 130 ± 2 mJ, and pulse duration of 7 ns was focused to a spot of about 200 μm onto the blood plasma samples by means of an air-spaced doublet lens with focal length of 30 mm. The laser beam was perpendicularly aligned to the target surface within a chamber (SciTrace, AtomTrace) kept at atmospheric pressure. Plasma emission was collected using an Echelle spectrometer

(Andor Technology, ME 5000) with a spectral range from 200 nm to 900 nm, coupled to a thermoelectrically cooled iStar Intensified Charge Coupled Device (ICCD) camera (Andor Technology, DH734-18F-03) through a 50 μm core-diameter optical fiber, at an angle of 45° with respect to the normal of the sample surface. To thermally stabilize the Echelle spectrometer, we placed the instrument in a thermally controlled Styrofoam chamber with a PID-controlled heater and an exhaust system. This enclosure effectively maintained the temperature of the Echelle constant to better than $\pm 1^\circ\text{F}$. We performed wavelength calibrations spanning the wavelength range 200–800 nm, emitted by an Hg-Ar pen lamp and directed into the same collection fiber used for LIBS data collection.

The spectra were collected at a delay time of 1500 ns and a gate width of 3000 ns which minimized self-absorption and saturation effects of the intensities of the emission lines. Collection of the LIBS spectra was performed with the negative, positive, and blind samples randomly placed on the Si substrate. For each sample, the collected spectra are the average of 15 shots at 4 different target positions, i.e., the average of 60 accumulated spectra. This reduces statistical fluctuations and compensates for any inhomogeneities in the liquid distribution on the substrate. Finally, we note that we have checked for any sign of saturation of the main emission lines (Na, K and Ca, Mg) and found none. In our LIBS spectra, the emission lines of these blood metals were clearly identified above the background and not saturating. Therefore, we are confident that the intensities of the various emission lines analyzed are proportional to the concentrations of the blood metals that produce them.

2.3. Data processing

The LIBS spectra acquired needs to be processed to reduce the contributions from noise caused by various experimental effects that affect LIBS reproducibility such as laser energy fluctuations, and inhomogeneities in the samples [37–39]. One such contribution can arise from the background continuum that may not be uniform in intensity across the spectral window of interest. Therefore, continuum background must be determined dynamically from spectra to spectra and from sample to sample. However, in our study, under the specified gating conditions, just as is the case in the LIBS spectra of biological samples, the background continuum energy of the plasma samples is significantly lower compared to that of the remaining spectra [36]. For the purpose of this study, it can be safely disregarded.

Visual inspection of the 60 spectra collected from each plasma sample revealed that the first spectra of every set of 15-shots per sample have low intensities, most likely due to surface contamination of the samples. These shots were eliminated from further analysis. The total sum of the measured intensities of the remaining 56 remaining spectra were subjected to a Z-score equal to 1.0 analysis. We selected a Z-score of 1 to tighten the range of intensities for the spectra measured for each patient. Spectra that had Z-scores higher than 1 were eliminated from further analysis. Using this procedure, we were left with between 30 and 51 spectra for each patient. These were used to calculate a mean spectrum for each patient. We then normalized each mean spectrum obtained by dividing its intensity by the total sum of the measured spectral intensities. This approach provided a normalized mean spectrum for each patient.

Next, we calculated the integral elemental spectral line intensities by selecting wavelength ranges that include the emission lines of interest while avoiding interference from adjacent spectral lines. Due to minor variations in line widths of the emission lines, the selected ranges also varied. Although the background continuum measured was low, we observed the presence of an underlying pedestal within the selected wavelength regions. To approximate this pedestal, we employed a trapezoid model using four points of the spectrum: the two limits of the wavelength ranges, the zero line of the spectral intensity and the specific spectral line. Using Simpson's rule, we determined the total line area under the curve contained between the limits of the wavelength

ranges and then subtracted the trapezoidal area of the underlying pedestal. This process yielded a normalized area under the curve (AUC) of the emission lines free of any visible background.

To facilitate comparison of the LIBS spectra of the samples collected, we introduce the notion of a “standard” covid-19 free donor. Utilizing plasma samples collected pre-Covid 19 pandemic, we calculated the mean value of each AUC for each of these samples. This mean value was then used to define the standard healthy patient. Subsequently, we compared to the AUC from all patients, including negative, positive, and blind to the AUC of the standard patient. This was performed by dividing the AUC of each patient by that of the mean of the standard covid-19 free donor. This implies that since the AUC of the LIBS spectra obtained pre-Covid-19 pandemic scatter around their mean values, the ratio of their AUC to that of the standard covid-19 free donor scatters around 1.

The experimental method and data processing procedure used in this study reduces the impact of laser energy fluctuations and of sample inhomogeneities but does not completely eliminate them. However, it provides a way to estimate the uncertainties associated with the intensities of the various emission lines which are represented by the error bars shown in Figs. 2, 3, and 4.

3. Results

3.1. Spectroscopic results of the negative and positive samples

In Fig. 1, we show an example of the mean normalized laser-induced spectrum of a donor known to have contracted Covid-19. Using a peak-finding algorithm and the NIST Atomic Spectra Database [40], we identified the most prominent atomic or ionic species i.e., with a relatively strong signal to noise ratio, responsible for the emitted spectral lines namely Si, Na, K, Ca, and Mg. We focused our current investigation on the emission lines of Na, K, Ca, and Mg, whereas Si emission lines were treated as contributors to the background from the Si wafer substrate used. Few spectra exhibited weak intensities associated with emission lines of Cu while emission lines of Fe were not considered in the present analysis due to coincidental emission at wavelength of elements.

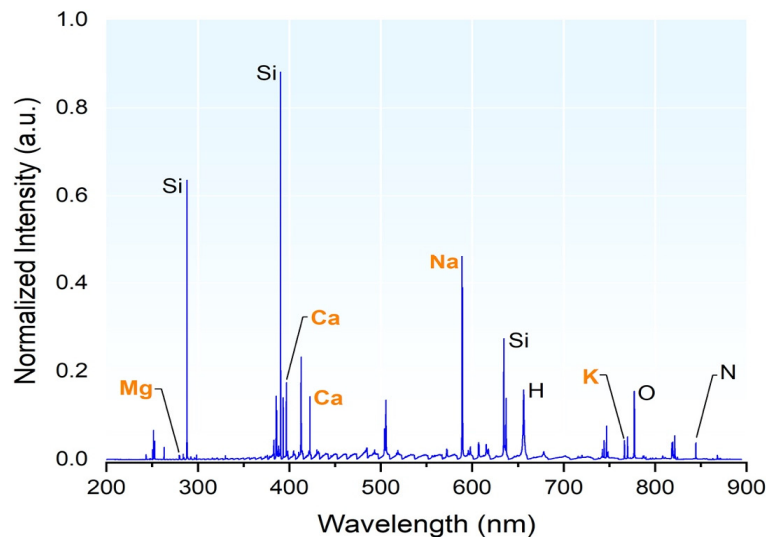


Fig. 1. The mean, normalized LIBS spectrum of a positive patient “Positive114”; out of initial 60 spectra measured, 41 remained after outlier removal.

To search for a pattern that can be used to distinguish between the negative and positive samples, we used a two-step approach. First, we compared AUCs of specific emission lines of

various blood metals measured for each donor. This step led to the identification of spectral features of the blood metals that may provide statistically significant differentiation between the negative and positive samples. Second, we systematically examined potential combinations of Na, K, Ca, and Mg using the logistic regression algorithm [41]. A summary for all 11 AUCs of the most prominent emission lines of K, Na, Mg and Ca is displayed in Fig. 2(a). To capture, a more representative behavior of the emission lines, we calculated the consolidated mean intensities with respect to healthy donors of the emission lines of Ca, K, Mg, and Na, for the negative and positive samples. This was obtained by adding the 4-, 2-, 3-, and 2- line areas displayed in Fig. 2(a) (for Ca, K, Mg, and Na respectively). Figure 2(b) displays the result of this process. We note that there is a statistically meaningful difference in the distributions of the emission lines of Ca, K and Mg, but it is not as pronounced for Na.

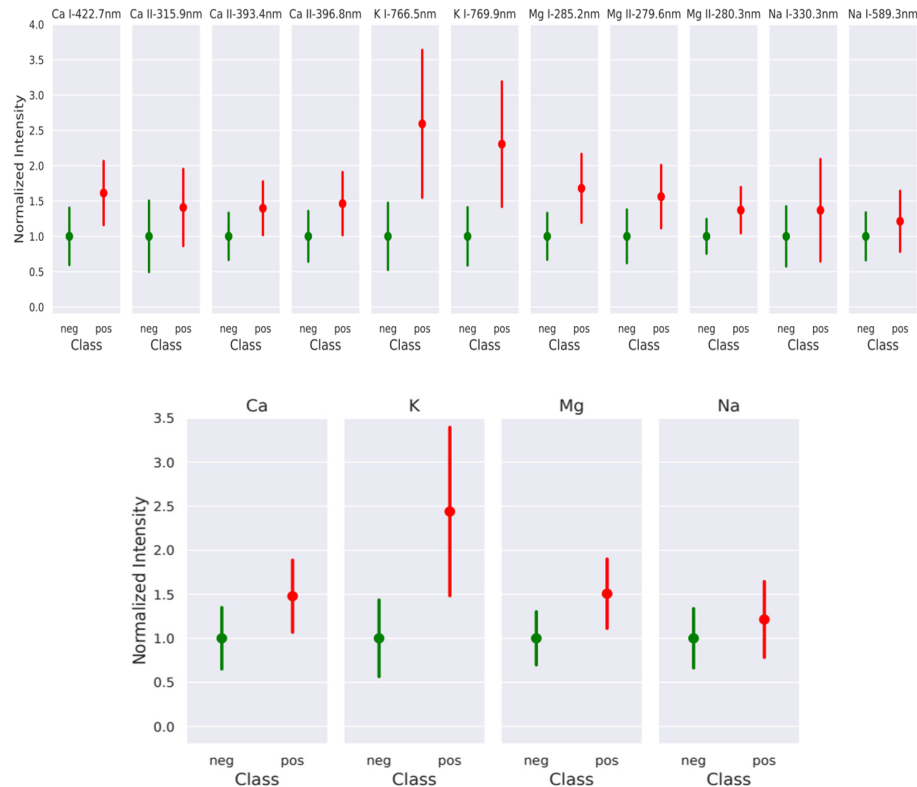


Fig. 2. a (top): Normalized Intensity with respect to negative samples (healthy controls) of the emission lines of Ca, K, Mg, and Na measured for each donor group: healthy controls (green) and patients infected with the corona virus (red). Figure 2(b) (bottom): Mean intensities with respect to healthy donors of the emission lines of Ca, K, Mg, and Na, measured for the negative samples (green) and for the positive samples (red).

Next, we attempted to distinguish between negative and positive samples using combinations of ratios and products of the intensities with respect to negative samples of the spectral emission lines of K, Na, Mg and Ca. As the number of possible combinations of these four elements is large, we have selected few that include K because it shows the largest separation between the negative and positive samples. The results of this analysis are shown in Fig. 3. We note that the results of a more rigorous approach that consider all possible combinations by taking advantage of tools from combinatorial mathematics are presented in Section 3.2.

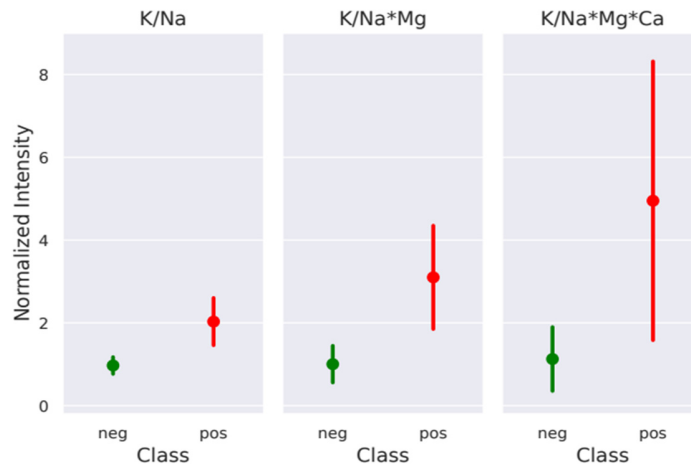


Fig. 3. Ratios of the normalized intensities of emission lines: K/Na, (K/Na) times Mg and (K/Na) times Mg times Ca of intensities with respect to negative samples (healthy controls). First, the value of each combination was calculated for every patient. Then, the mean and the standard deviation of these combination values were calculated for the negative and positive donor groups. The error bars represent one standard deviation from the mean.

To differentiate between the negative and positive plasma samples, we have calculated the intensity of the ratio of the emission lines of K and Na for each patient, including the samples that were blind to us. To do this, we have used the 766.5 nm and 769.9 nm emission lines of K and the 330.3 nm and 589.3 nm emission lines of Na, to determine the intensities of the area under the curves of the K/Na spectral emission for each patient. This is shown in Fig. 4. We note that we could have selected Mg as one additional element to include in the differentiation of the negative and positive samples but for simplicity we opted not to at this stage.

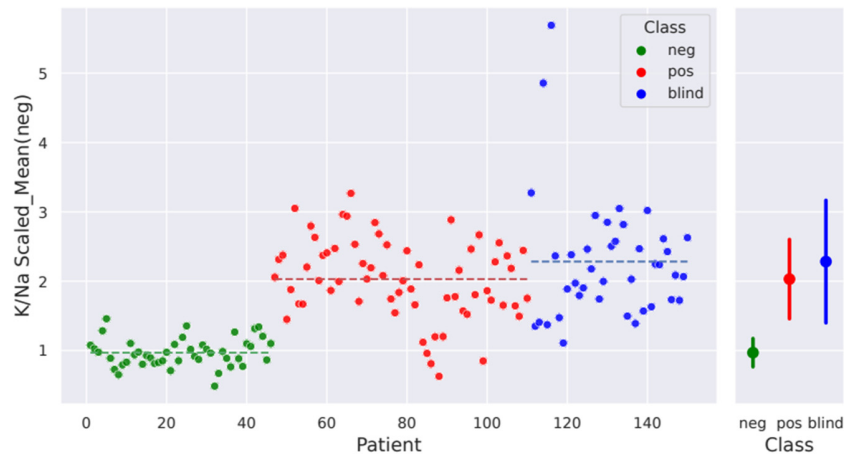


Fig. 4. Left panel: Intensity ratios K/Na with respect to negative samples (healthy controls) of the K and Na emission lines measured for each donor group: negative (green dots), positive (red dots), and blind samples (blue dots). The broken lines identify the positions of the mean value for each group. The error bar on the K/Na value for each patient is of the order of the one standard deviation of the mean shown in the right panel. **Right panel:** Mean of the data shown on the left panel of the negative (green), positive (red), and blind (blue dots) and the one standard deviation from the mean.

3.2. Logistic regression analysis of spectroscopic data of negative and positive samples

Based on the intensities of the spectral features shown in Figs. 1 and 2, the emission lines of Na, K, Mg, and Ca were selected to build the discrimination model. Further, to identify which of these 4 blood metals contribute the most to the differentiation of the spectra of plasma samples of healthy donors and positive, we use the logistic regression algorithm for training binary classifiers [42,43]. In this case, we consider a *training* data set comprising 30 healthy donors or negative samples and 30 diseased patients or positive samples. The feature space for each sample contains information about Na, K, Mg, and Ca. The logistic regression algorithm provides a probability score for each input by forming a weighted combination of the input features and applying the logistic or sigmoid function. Therefore, the main step during the training process is finding the unknown weights, which can be done by minimizing the cross-entropy loss function [44]. After finding these weights in the training stage, we can use logistic regression for predicting classes of new samples, i.e., positive vs. negative. Prior to using the algorithm, it is important to evaluate the resilience of the model established in the training phase. This step is necessary to assess the predictive efficacy of the model using evaluation metrics that can provide a quantitative assessment of the performance of the model. To do this we used metrics typically used for the evaluation of machine learning models [45,46]:

$$\text{Sensitivity} = \frac{TP}{TP + FN} \times 100 \quad (1)$$

$$\text{Specificity} = \frac{TN}{TN + FP} \times 100 \quad (2)$$

$$\text{Total accuracy} = \frac{TP + TN}{TP + TN + FP + FN} \times 100 \quad (3)$$

where TP = true positive (samples correctly classified as positive (Covid-19), FN = false negative (positive samples wrongly classified as negative (health controls), TN = true negative (samples correctly classified as negative), FP = false positive (negative samples wrongly classified as positive.)

Due to the small sample size, we evaluated the classification performance on the training data set using the leave-one-out cross-validation (LOOCV) [47,48]. To explain this process, the logistic regression algorithm is trained on all but one sample and then tested on the hold-out sample. Hence, this process should be repeated 60 times because there are 60 training samples: each time with 59 training samples and a single validation data point. To further assess the performance of the trained classifier, we also created a separate test or blind set. This set comprised the remaining 16 negative and 34 positive samples, resulting in a total of 50 samples. The purpose of this test/blind set is to measure how well the classifier performs on unseen data, which is known as data splitting in statistical and machine learning. In Fig. 5, we present two confusion matrices to discuss the performance of the logistic regression algorithm using the training and testing data sets. Each row of the confusion matrix corresponds to a true class while each column represents a predicted class. Based on the left panel in Fig. 5, the logistic regression algorithm achieves a classification accuracy of 88.33%, sensitivity of 90.00%, and specificity of 86.66%. On the other hand, using the testing/blind data set on the right panel of Fig. 5, the same process results in a classification accuracy of 82.00%, sensitivity of 79.41%, and specificity of 87.50%. Hence, compared to the training data set, the specificity of the logistic regression algorithm remains mostly the same, whereas the sensitivity drops by almost 10%. This reduction is the result of the increase in the number of false negatives from 3 to 7, which is small when compared to the total number of positive samples in both training and testing data sets.

To account for the potential impact of data splitting on our results, we conducted a more comprehensive analysis by performing ten independent trials. In each trial, we randomly split the

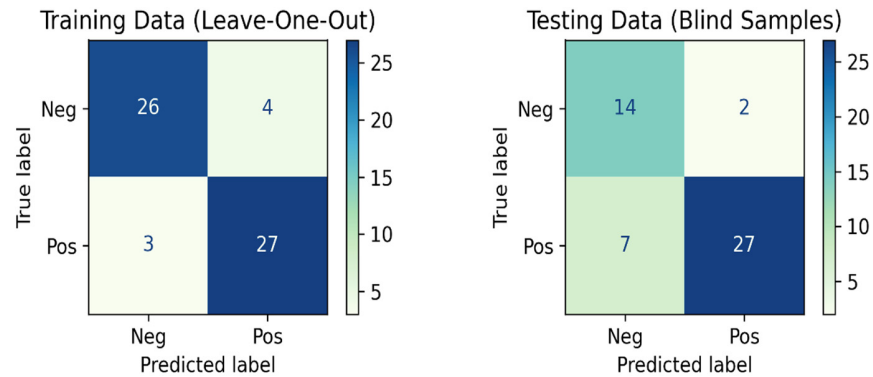


Fig. 5. Left panel: Confusion matrix for the entire set of 30 negative and 30 positive samples or the training data set (obtained using leave-one-out cross-validation). Right panel: Confusion matrix for testing/blind data set comprising 16 negative and 34 positive samples (obtained using data splitting).

available data into training and testing sets, ensuring a diverse range of data configurations. For each trial, we calculated the evaluation metrics and observed the range of values obtained across all trials. Specifically, the classification accuracy varied from 82% to 94%, demonstrating the performance range of our model. Additionally, the sensitivity ranged from 79.41% to 94.11%, indicating the variation in correctly identifying positive instances. Similarly, the specificity

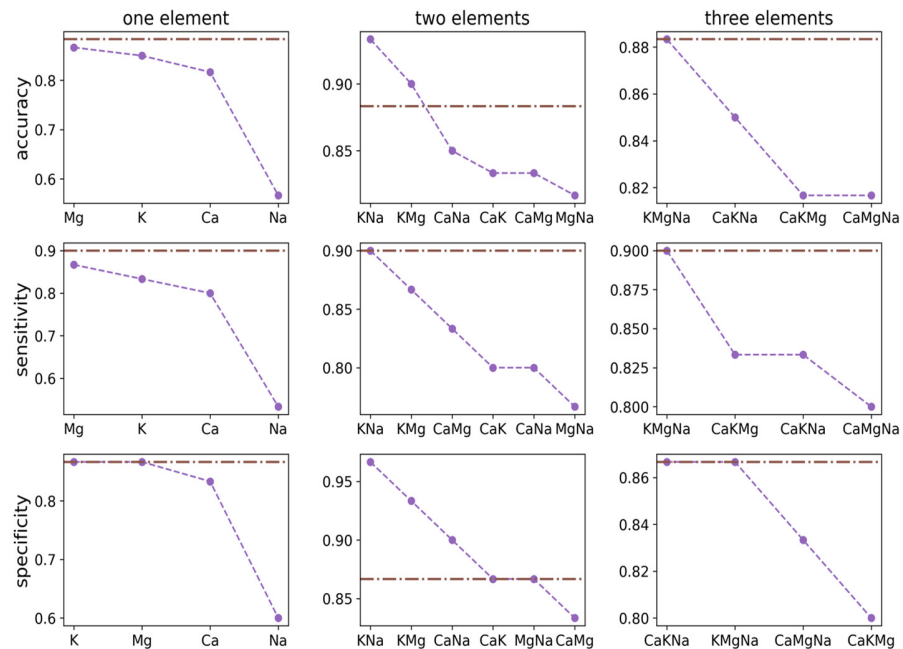


Fig. 6. Accuracy, sensitivity, and specificity for varying subsets of the chemical set (Na, K, Mg, Ca). Each row corresponds to one metric and each column corresponds to the specific number of blood metals considered in the evaluation of the performance metrics of the training model: one, two and three blood metals. The horizontal line in each figure represents the corresponding performance metrics obtained by using Na, K, Mg, and Ca.

showed a range of values between 81.25% and 93.75%. Therefore, our analysis reveals that the logistic regression algorithm performs reasonably well in terms of identifying positive samples, which is necessary for our next analysis to examine the interrelationship between blood metals and their influence on the classification performance.

To this end, we consider all possible combinations of the blood metal signals measured (Na, K, Mg, Ca) using tools from combinatorial mathematics. We start by finding all possible ways to form subsets of varying sizes, from one blood metal to the total number of elements in the chemical set. We then train the logistic regression algorithm using each subset and assess its performance by reporting various metrics, such as sensitivity and specificity, using leave-one-out cross-validation on the training data set. In addition, we sort these measures in descending order to find the optimal size and combination of the blood metals. Based on the first column of Fig. 6, we see that using a single blood metal is not sufficient for reaching the performance of the baseline classifier trained using the emission lines of Na, K, Mg, and Ca. Moreover, using Na, K, Mg as the feature set for training the logistic regression algorithm results in higher accuracy and specificity levels compared to using the emission lines of Na, K, Mg, and Ca. This suggests that the levels Na, K, Mg are again shown to be the main differentiator between the negative and positive samples.

4. Discussion

Alterations of levels of bio metals in blood have been reported by several research groups. However, the association of individual bio metal on how the disease manifest itself are inconsistent. Both higher and lower levels of Na, K, Ca, and Mg in blood of Covid-19 patients have been reported [5–9]. This observation suggests the need for a multi bio metal study. Investigating association of each blood metal with Covid-19 separately from others may not be sufficiently effective to differentiate healthy donors from Covid-19 patients. In doing so, this study reveals several findings.

First, among healthy donors, the intensity of all the emission lines considered were less scattered than those of the donors infected with the SARS-Cov-2 virus and the mean of the K, Na, Mg and Ca emission lines of the positive samples was higher than those measured of the negative controls (Fig. 2). The largest difference between the emission lines of the plasma samples of negative controls and the positive samples was from K, followed by Mg, Ca, and Na. We then evaluated the ratio of the normalized intensities of the emission lines of K/Na, $(K/Na) \times Mg$ and $(K/Na) \times (Mg \times Ca)$. As shown in Fig. 3, the ratios K/Na and $(K/Na) \times Mg$ provide statistically significant differentiations between the negative and positive samples that are larger than if K or Na are considered separately. Other studies have shown that this ratio plays a significant role in several diseases (e.g., high blood pressure, heart disease) [49,50]. These results highlight the potential of using a multi-elemental analysis approach instead of a single bio-metal approach. In this way, combinations of blood metals might not be lost by individual variability, allowing the emergence of distinct processes.

Second, as can be observed from Fig. 4, we found that the LIBS signatures of the negative samples to be more stable than those of the positive samples. Despite the scattering of values around the mean of the negative and positive donors, there is a statistically significant difference in the areas of the intensities of the K/Na emission lines of the negative and positive samples. Next, we sought to use K/Na intensity ratios to determine if each blind plasma sample was negative or positive. This revealed that about 80% of the blind samples were positive. We have tested this result by subsequently measuring the SARS-CoV-2 antibody levels of the all the samples using the LumiraDx SARS-CoV-2 antigen microfluidic immunofluorescence assay targets total antibodies test. We found that the LIBS and the antigen microfluidic immunofluorescence assay show that more than 85% of the blind samples were positive. The results of this part of this study will be the subject of a forthcoming manuscript that will focus on the relationship between the

blood metals and the SARS-CoV-2 antigen measured using the SARS-CoV-2 antigen microfluidic immunofluorescence assay.

We note that this is not a longitudinal study based on each patient, but one performed on a group of donors with different levels of severity to Covid-19. The blood donations occurred in an area where there were several Covid-19 variants in circulation during the donor blood collections [51]. Previously, we investigated the antibody decay rates among the same convalescent Covid-19 patients who were part of the same Mayo Clinic EAP Trial and estimated the length of time they maintained SARS-CoV-2 specific antibodies over the course of 7 months, with a gradual decrease of the IgG levels among the donors [52]. Dan *et al.* reported that the levels of antibody from Covid-19 infected patients were present within 2 weeks of clearance of symptoms, and that the immunological memory to SARS-CoV-2 could last 8 months [53]. This study also reports on a change lingering post infection but in a process linked to the K/Na ratio. Potassium and Na have been implicated in studies that showed that patients infected with SARS-CoV2 had an electrolyte imbalance [18]. This ratio, controlled by the Na, K-ATPase, is found to be likely disturbed in donors who contracted Covid in line with recent findings that show that both influenza and SARS-CoV-2 negatively impact the Na, K-ATPase in the lungs [54]. Furthermore, a recent study reports on the significance of maintaining a balanced level of Mg and suggests that Mg homeostasis in Covid-19 and that serum Mg levels might play a role in the pathogenesis of Covid-19 [12]. Our findings suggest that although LIBS does not measure antibody levels, it provides information on an unidentified chemical change in the blood of infected patients that lingers after the infectious stage is passed.

Third, the results of the logistic regression analysis using spectral features of K, Na, Ca, and Mg show that by using various combinations of data sets, we found that the classification accuracy varied from about 82% to about 94%, demonstrating the performance range of our model. Additionally, the sensitivity ranged from 79.41% to 94.11%, indicating the variation in correctly identifying positive instances. Similarly, the specificity showed a range of values between 81.25% and 93.75%. In addition, as shown in Fig. 6, the classification performance metrics are higher when combinations of two, three or all the four blood metals are considered rather than any alone and that (see middle column), the specificity obtained with K and Na, is higher than that obtained with one, three or four bio-metals. We also note that Mg combined with Na, and K yields contributes significantly to the differentiation albeit slightly less than the K, Na combination alone. Figure 6, shows that the Mg, K combination contributes significantly to the differentiation (accuracy of 90%) albeit slightly less than the K, Na combination (accuracy of about 94%) and when we combine all three elements, Na, K, and Mg, the accuracy of the differentiation diminishes to about 88%. This suggests that subtle variations in the relationship between the concentrations of multiple bio metals are implicated in the blood plasma of individuals with Covid-19, particularly the ratio of K to Na. These two blood metals outperform any other combinations of Na, K, Mg, and Ca in our classification of blood samples possibly because the normal concentrations of Na (140 mmol/L) and K (mmol/L) are much higher than those of Ca (2 mmol/L) and Mg (0.25 mmol/L). We expect that although these four blood metals are involved in many physiological processes, K and Na may be more essential than any other blood metal combinations; K and Na are known to play a significant role in regulating blood pressure and maintaining cell integrity.

5. Conclusions

This work shows that combinations of multiple blood metals, K, Na, and Mg, more than any of these by itself, distinguishes blood plasma samples from healthy patients and those who have contracted the corona virus. Combinations of blood metals provide higher accuracy, specificity, and sensitivity in the classification of the spectra of the blood plasma samples than any blood metal considered alone. To our knowledge, this is the first study conducted on the levels of blood

metals in COVID-19 patients that considers combinations of multiple blood metals measured simultaneously in plasmas collected pre- and post-pandemic. This study suggests the potential presence of subtle interactions of the bio-metals on the status of Covid-19 donors. These can aid the understanding of the underlying biochemical processes that have been altered after infection with SARS-CoV-2 or in other diseases [17,18]. However, to identify the combinations of blood metals that yield the highest differentiation, we have performed a logistic regression analysis. This approach provides information on whether a specific sample originates from a healthy or a diseased donor. No information on the severity or any other aspect of the disease can be inferred from our study. In addition, we have shown that the ratio of the LIBS emission lines of K/Na changes by about 2 between negative and positive samples suggesting that it may indirectly reflect patient antibody status. There may be other factors that contribute to the differentiation between the samples from donors with and without SARS-CoV-2. However, despite this possibility, as this study yields high accuracy of differentiation, we suspect that it has the potential to contribute to elucidate the role of blood metals in Covid-19 patients.

We envisage that future studies focus on the relationship between the blood metals shown to contribute to the differentiation of healthy donors and Covid-19 patients with the level of SARS-CoV-2 antibody in plasma. It is likely that a longitudinal study that will measure the levels of multiple blood metals in plasma samples periodically over several months, and possibly years, in the same patient be useful. It may establish whether the observed change in blood metals (Fig. 4) persists as patients initially diagnosed with Covid-19 recover and become healthy. Such a study can contribute to a better understanding of the prevalence of covid-19 over time. In addition, future studies may incorporate our analysis of metal spectra into T-cell system and other aspects of the immune system that likely contribute to the immunity response and protection against the variants of Covid-19 [55]. Understanding the human immune response to infection by various variants, vaccination and breakthrough infections after vaccination are critical to understanding the waning protection of humoral immunity, vaccinations, vaccine booster timing, and herd immunity. The simultaneous multi-elemental analytical information that LIBS provides is a new perspective that opens the possibility of enhancing our readiness and preparation for future pandemics.

Disclosures. The authors declare no conflicts of interest.

Data Availability. The data collected for this study is available without any restriction. It can be accessed at [56].

Supplemental document. See [Supplement 1](#) for supporting content.

References

1. www.who.int/publications/m/item/weekly-epidemiological-update-on-covid-19—18-may-2022
2. M. Szmigiera, "Impact of the coronavirus pandemic on the global economy-Statistics & Facts," Accessed Sep 17 (2021).
3. Holly. Else, "Covid in papers," *Nature* **588**(7839), 553 (2020).
4. A. V. Skalny, P. S. Timashev, M. Aschner, *et al.*, "Serum zinc, copper, and other biometals are associated with Covid-19 severity markers," *Metabolites* **11**(4), 244 (2021).
5. M. Noori, S. A. Nejadghaderi, M. J. M. Sullman, *et al.*, "Epidemiology, prognosis and management of potassium disorders in Covid-19," *Rev. Med. Virol.* **32**(1), e2262 (2022).
6. F. Yasari, M. Akbarian, A. Abedini, *et al.*, "The role of electrolyte imbalances in predicting the severity of COVID-19 in the hospitalized patients: a cross-sectional study," *Sci Rep* **12**(1), 14732 (2022).
7. T. Hoca N and B. M. Berktaş, "Baseline electrolyte disorders predict disease severity and mortality in patients with COVID-19," *Medicine* **101**(51), e32397 (2022).
8. H. J. J. M. D. Song, A. Z. Q. Chia, B. K. J. Tan, *et al.*, "Electrolyte imbalances as poor prognostic markers in COVID-19: a systemic review and meta-analysis," *J. Endocrinol. Invest.* **46**(2), 235–259 (2022).
9. G. Lippi, A. M. South, and B. M. Henry, "Electrolyte imbalances in patients with severe coronavirus disease 2019 (COVID-19)," *Ann. Clin. Biochem.* **57**(3), 262–265 (2020).
10. Oliver Micke, Jürgen Vormann, and Klaus Kisters, "Magnesium deficiency and Covid-19 – What are the links? Some remarks of the German society for magnesium research," *Trace Elements and Electrolytes* **37**(07), 103–107 (2020).
11. V. Trapani, A. Rosanoff, S. Baniyadi, *et al.*, "The relevance of magnesium homeostasis in COVID-19," *Eur. J. Nutr.* **61**(2), 625–636 (2022).

12. S. Iotti, F. Wolf, A. Mazur, *et al.*, "The COVID-19 pandemic: is there a role for magnesium? Hypotheses and perspectives," *Magnesium Research* **33**(2), 21–27 (2020).
13. Shahnaz Fooladi, Somaieh Matin, and Ata Mahmoodpoor, "Copper as a potential adjunct therapy for critically ill COVID-19 patients," *Clinical Nutrition ESPEN* **40**, 90–91 (2020).
14. V. Chinni, E. J. Perera, M. Perera, *et al.*, "Zinc supplementation as an adjunct therapy for COVID-19: Challenges and opportunities," *Br J Clin. Pharmacol.* **87**(10), 3737–3746 (2021).
15. M. K. Sobczyk and T. R. Gaunt, "The effect of circulating zinc, selenium, copper and vitamin K₁ on COVID-19 Outcomes: A Mendelian Randomization Study," *Nutrients* **14**(2), 233 (2022).
16. J. Alexander, A. Tinkov, T. A. Strand, *et al.*, "Early nutritional interventions with zinc, selenium and vitamin d for raising anti-viral resistance against progressive Covid-19," *Nutrients* **12**(8), 2358 (2020).
17. H. Sarvazad, S.H. Cahngaripour, N. Eskandari Roozbahani, *et al.*, "Evaluation of electrolyte status of sodium, potassium and magnesium, and fasting blood sugar at the initial admission of individuals with COVID-19 without underlying disease in Golestan Hospital, Kermanshah," *New Microbes and New Infections* **38**, 100807 (2020).
18. D. Chen, X. Li, Q. Song, *et al.*, "Assessment of hypokalemia and clinical characteristics in patients with coronavirus disease 2019 in Wenzhou, China," *JAMA network open* **3**(6), e2011122 (2020).
19. O. F. Kocak, F. B. Ozgeris, E. Parlak, *et al.*, "Evaluation of serum trace element levels and biochemical parameters of Covid-19 patients according to disease severity," *Biol Trace Elem Res* **200**(7), 3138–3146 (2022).
20. Tamer Bego, Neven Meseldžić, Besim Prnjavorac, *et al.*, "Association of trace element status in COVID-19 patients with disease severity," *J. Trace Elem. Med. Biol.* **74**, 127055 (2022).
21. K. Berlo, W. Xia, F. Zwilllich, *et al.*, "Laser induced breakdown spectroscopy for the rapid detection of SARS-CoV-2 immune response in plasma," *Sci. Rep.* **12**(1), 1614 (2022).
22. I. Goodfellow, Y. Bengio, and A. Courville, "Machine-learning models trained on larger data sets are known to be more accurate, generalizable, and less prone to overfitting," in *Deep Learning* (MIT Press, 2016).
23. R. Gaudiuso, S. Chen, E. C. Kokkotou, *et al.*, "Diagnosis of Gulf War Illness Using Laser-Induced Spectra Acquired from Blood Samples," *Appl. Spectrosc.* **76**(8), 887–893 (2022).
24. R. Gaudiuso, E. Ewusi-Annan, X. Weiming, *et al.*, "Diagnosis of Alzheimer's disease using laser induced breakdown spectroscopy and machine learning," *Spectrochim. Acta, Part B* **171**, 105931 (2020).
25. D. Zhang, H. Zhang, Y. Zhao, *et al.*, "A brief review of new data analysis methods of laser-induced breakdown spectroscopy: machine learning," *Appl. Spectrosc. Rev.* **57**(2), 89–111 (2022).
26. Xue Chen, Xiaohui Li, Xin Yu, *et al.*, "Diagnosis of human malignancies using laser-induced breakdown spectroscopy in combination with chemometric methods," *Spectrochimica Acta Part B: Atomic Spectroscopy* **139**, 63–69 ISSN 0584-8547 (2018).
27. Q. Wang, G. Teng, X. Qiao, *et al.*, "Importance evaluation of spectral lines in Laser-induced breakdown spectroscopy for classification of pathogenic bacteria," *Biomed. Opt. Express* **9**(11), 5837–5850 (2018).
28. Z. Yue, C. Sun, F. Chen, *et al.*, "Machine learning-based LIBS spectrum analysis of human blood plasma allows ovarian cancer diagnosis," *Biomed. Opt. Express* **12**(5), 2559–2574 (2021).
29. K. McCance, H. Wise, J. Simpson, *et al.*, "Evaluation of SARS-CoV-2 antibody point of care devices in the laboratory and clinical setting," *Plos one* **17**(3), e0266086 (2022).
30. Miziolek Andrzej W., Vincenzo Palleschi, and Israel Schechter, eds. *Laser-induced Breakdown Spectroscopy* (Cambridge University Press, 2006).
31. S. Musazzi and U. Perini, "Laser-induced breakdown spectroscopy," Springer Series in Optical Sciences 182 (Springer, 2014).
32. J. D. Winefordner, I. B. Gornushkin, T. Correll, *et al.*, "Smith and Nicolo ´ Omenetto; Comparing several atomic spectrometric methods to the super stars: special emphasis on laser induced breakdown spectrometry, LIBS, a future super star," *J. Anal. At. Spectrom.* **19**(9), 1061–1083 (2004).
33. N. Melikechi, Editor, *Optical spectroscopy and imaging: Fundamentals, Progress and Challenges* (World Scientific Publishing Inc. Singapore, WSP, 2023) and references therein.
34. N. Melikechi, Y. Markushin, D. Connolly, *et al.*, "Age specific classification of discrimination of blood plasma samples of healthy and ovarian cancer prone mice using laser-induced breakdown spectroscopy," *Spectrochimica Acta Part B Atomic Spectroscopy* **123**, 33–41 (2016).
35. Y. Markushin, P. Sivakumar, D. Connolly, *et al.*, "Tag-Femtosecond Laser Induced Breakdown Spectroscopy for the Sensitive Detection of Cancer Antigen 125 in Blood Plasma," *Anal. Bioanal. Chem.* **407**(7), 1849–1855 (2015).
36. A. Metzinger, É. Kovács-Széles, I. Almási, *et al.*, "An Assessment of the Potential of Laser-Induced Breakdown Spectroscopy (LIBS) for the Analysis of Cesium in Liquid Samples of Biological Origin," *Applied Spectroscopy* **68**(7), 789–793 (2014).
37. I. B. Gornushkin, P. E. Eagan, A. B. Novikov, *et al.*, "Automatic Correction of Continuum Background in Laser-Induced Breakdown and Raman Spectrometry," *Appl. Spectrosc.* **57**(2), 197–207 (2003).
38. V. Lazic, R. Fantoni, A. Palucci, *et al.*, "Sample Preparation for Repeated Measurements on a Single Liquid Droplet Using Laser-Induced Breakdown Spectroscopy," *Appl. Spectrosc.* **71**(4), 670–677 (2017).
39. Vincenzo Palleschi, Editor, *Chemometrics and Numerical Methods in LIBS* (John Wiley & Sons Ltd., 2023), and references therein.
40. A. Kramida, Yu. Ralchenko, and J. Reader and NIST ASD Team (2022). NIST Atomic Spectra Database (version 5.10).

41. David D. Pokrajac, "Cancer diagnosis using optical methods: Fundamentals of classification with machine learning.," In *Optical Spectroscopy and Imaging for Cancer Diagnostics: Fundamentals, Progress, and Challenges*, pp. 99–135. 2023.
42. Y. Yang and M. Loog, "A benchmark and comparison of active learning for logistic regression," *Pattern Recognition* **83**, 401–415 (2018).
43. M. S. Dekka, K. N. Raju, D. ManendraSai, *et al.*, "Utilizing Machine Learning Algorithms For Kidney Disease Prognosis," *European Journal of Molecular & Clinical Medicine* **10**(01), 1 (2023).
44. F. Pourkamali-Anaraki and M. A. Hariri-Ardebili, "Neural networks and imbalanced learning for data-driven scientific computing with uncertainties," *IEEE Access* **9**, 15334–15350 (2021).
45. Vera Sitnikova, Tatina Nosenko, and Mayya Uspenskaya, "Application of ATR-FTIR spectroscopy to the study of blood sera of patients with breast cancer," in "*Optical spectroscopy and imaging: Fundamentals, Progress and Challenges*" (World Scientific Publishing Inc. Singapore, WSP, 2023).
46. Michael Greenop, Carlos A. Meza Ramirez, and Ihtesham Ur Rehman, "Raman Spectroscopy and machine learning for diagnosis and monitoring of cancer," in "*Optical spectroscopy and imaging: Fundamentals, Progress and Challenges*" (World Scientific Publishing Inc. Singapore, 2023).
47. Xingjun Ma, Hanxun Huang, Yisen Wang, *et al.*, "Normalized loss functions for deep learning with noisy labels.," In *International conference on machine learning* 6543–6553. PMLR, (2020).
48. T.-T. Wong, "Performance evaluation of classification algorithms by k-fold and leave-one-out cross validation," *Pattern Recognition* **48**(9), 2839–2846 (2015).
49. M. Lucarini, A. Durazzo, S. Sette, *et al.*, "Sodium Intake and Related Diseases," *Int. J. Mol. Sci.* **22**(14), 7608 (2021).
50. M. Kogure, N. Nakaya, T. Hirata, *et al.*, "Sodium/potassium ratio change was associated with blood pressure change: possibility of population approach for sodium/potassium ratio reduction in health checkup," *Hypertens Res* **44**(2), 225–231 (2021).
51. TJ Hladish, AN Pillai, IM. Toh, *et al.*, *Projections for COVID-19 delta wave in Florida*. University of Florida 2021.
52. W Xia, M Li, Wang, *et al.*, "Longitudinal analysis of antibody decay in convalescent COVID-19 patients.," *Sci Rep.* **11**(1), 16796 (2021).
53. J Dan, J Mateus, C Kato, *et al.*, "Immunological memory to SARS-CoV-2 assessed for up to 8 months after infection.," *Science*. **371**(6529), 6 (2021).
54. V Kryvenko and I. Vadasz, "Molecular mechanisms of Na,K-ATPase dysregulation driving alveolar epithelial barrier failure in severe COVID-19.," *Am J Physiol Lung Cell Mol Physiol* **320**(6), 3206L1186 (2021).
55. H. Ledford, "'Killer' immune cells still recognize Omicron variant," *Nature [News]* **601**(7893), 307 (2022).
56. A. Safi, N. Melikechi, H. Adler, *et al.*, "Laser spectra of covid and non-covid blood samples," figshare (2023).<https://doi.org/10.6084/m9.figshare.24260911.v2>